Available online at www.sciencedirect.com
SCIENCE DIRECT®
Journal of Nuclear Materials 334 (2004) 195–199
journal of nuclear materials
www.elsevier.com/locate/jnucmat

Multi-component clustering in VVER-type pressure vessel steels – thermodynamic aspects and impact on SANS

A. Gokhman, J. Böhmert, A. Ulbricht *

Forschungszentrum Rossendorf, Institut für Sicherheitsforschung, P.O. Box 510119, D-01314 Dresden, Germany

Received 10 October 2003; accepted 17 June 2004

Abstract

Atom probe field ion microscopic investigations of irradiated VVER 440-type reactor pressure vessel steels suggest the appearance of multi-component clusters. The effect is unexpected considering the phase diagrams of the concerning alloys. Numerical calculations of the negative minimum of the thermodynamic driving forces for a multi-component system are carried out considering a quasi-quaternary system consisting of Fe, Mn, Si and vacancies. A relative minimum was only found for a composite model of the multi-component clusters composed of an Fe containing core and a vacancies-rich shell. The ratio of their sizes is estimated from the condition that such structures agree with the small-angle neutron scattering (SANS) curves measured.

1. Introduction

Mechanism and sequence of the microstructural damage processes in the ferritic reactor pressure vessel steels due to neutron irradiation are complex, diverse and multi-graded. Two types of features have primarily been taken into account: copper-rich precipitates (CRP) and small point defect clusters (PDC) of not identified nature, also named matrix defects [1–7]. The first feature is radiation-enhanced and appears in steels with higher contents of copper and already after low fluences whereas the second type dominates in low-copper steel and after high neutron fluence and arises from irradiation-induced effects. Surprisingly, both features exhibit the same or a very similar size distribution with a clearly pronounced peak near a radius of approximately 1 nm. Related to the small-angle neutron scattering (SANS) effects, there is only a difference in the ratio between the total and the nuclear scattering section (the so-called A-ratio) [8]. This ratio is high for steels with high Cu content and low for Cu-poor steels.

However, the results from field emission gun scanning transmission electron microscopy (FEGSTEM) [9–11] and, above all, atom probe field ion microscopy (APFIM) [12–18] are not or not sufficiently consistent with this approach. Here, especially in RPV steels with low Cu content, the defects are identified as local solute enrichments of silicon, manganese, nickel and copper or even phosphorus within the ferrite solid solution. There is no clear interface between the matrix and defects, and the composition varies strongly. Cu is characterized by a high enrichment compared with the matrix content but

* Corresponding author. Tel.: +49 351 260 3155/4; fax: +49 351 260 2205.
E-mail address: a.ulbricht@fz-ssendorf.de (A. Ulbricht).

0022-3115/$ - see front matter © 2004 Elsevier B.V. All rights reserved.
doi:10.1016/j.jnucmat.2004.06.008

does not often exceed some percent on the absolute scale. The features are rather cloud-like. Unfortunately, the content of vacancies cannot be measured by APFIM. Similar results were obtained on VVER-type RPV weld and base metal [19,20].

The evolution of such multicomponent clusters (MCC) is rather unexpected from the thermodynamic point of view. Under temperature controlled conditions such precipitates do not occur and the content of Ni, Mn or Si lies far within the solubility limit for the temperature concerned. Odette [4] gives a thermodynamic explanation for Ni alloyed RPV steels considering the significant contribution of the composition-dependent interface energy to the total molar Gibbs energy in the case of very fine, nanoscaled radiation defects. However, the basis remains the Cu precipitation as initiating process.

The paper presents thermodynamic considerations on the formation of MCC in VVER-type RPV steels. The small angle neutron scattering effects resulting from the thermodynamic estimation of MCCs are calculated and compared with experimental results.

2. Thermodynamics of the MCC in steel

From the thermodynamic point of view, the formation of inhomogeneities in the steel after the cascade stage is ruled by changing of the Gibbs energy (ΔG), and can be described in accordance with [21–23] by Eq. (1)

$$\Delta G = nk_{\mathrm{B}}Tf(x_1, x_2, \ldots x_k/x'_1, x'_2, \ldots, x'_k) + A\sigma, \tag{1}$$

n is the total number of atoms in MCC; f is so-called thermodynamic driving force (TDF); $(x_1, x_2, \ldots, x_k)$ and $(x'_1, x'_2, \ldots, x'_k)$ are the fractions of the $1, 2, \ldots k$ kinds of atoms in the solution (matrix) and MCC, respectively; k_{B} is the Boltzmann constant and T is the temperature in K; A is the surface area and σ is the surface tension.

A phase separation may occur in the system if the TDF is negative at least for certain of the variables of x_n, x'_n. Moreover, in [23] it is found that for small supersaturations the classical Gibbs approach is fulfilled, i.e. the composition of the critical cluster has values near the binodal curve and with an increase of the initial concentration of the solute, the highest driving force for the transformation are located at values of solute concentration which are larger than the value for the evolving macrophase.

As a result of the generalization of the formula for TDF for binary alloy in [23] on the case of multicomponent alloys, Eq. (2) is deduced

$$\begin{aligned} f(x_1, x_2, \ldots, x_k/x'_1, x'_2, \ldots, x'_k) &= x'_1[\ln(x'_1/x_1) + (w_{1,2}/k_{\mathrm{B}}T)(x'^2 - x_2^2) + \cdots \\ &+ (w_{1,k}/k_{\mathrm{B}}T)(x'^2_k - x_k^2)] + x'_2[\ln(x'_2/x_2) \\ &+ (w_{1,2}/k_{\mathrm{B}}T)(x'^2_1 - x_1^2) + \cdots + (w_{2,k}/k_{\mathrm{B}}T)(x'^2_k - x_k^2)] \\ &+ \cdots + x'_k[\ln(x'_k/x_k) + (w_{k,1}/k_{\mathrm{B}}T)(x'^2_1 - x_1^2) + \cdots \\ &+ (w_{k,(k-1)}/k_{\mathrm{B}}T)(x'^2_{k-1} - x_{k-1}^2)]. \end{aligned} \tag{2}$$

Here $w_{i,j}$ is the interchange energy (or mixing energy with inverse sign) for atoms of the i- and j-kinds and is connected with the transition temperature $T_{\mathrm{c}}(i,j)$ of the first-order transformation:

$$w_{i,j} = 2k_{\mathrm{B}}T_{\mathrm{c}}(i,j). \tag{3}$$

It is easy to prove that Eq. (2) corresponds to a special case of the Eq. (2.23) in [24] when the binary approximation is considered, i.e. the total energy interaction is presented as a sum of the interaction between different pairs of atoms only and consequently the ternary and other impacts of the multiparticle interaction are not considered.

MCC formation only occurs for those fixed compositions of the elements in the matrix and MCCs that provide the negative minimum of the TDF function. This problem is simple from the calculation point of view but values of $w_{i,j}$ for a set of components in the matrix and MCCs are not well-known for irradiated condition. Therefore, in the present paper one fitting parameter T_{c} is used as rough estimation of $T_{\mathrm{c}}(i,j)$ for all pairs in Eq. (2). This means that instead of the real multiparticle interaction, the binary interaction model with one effective parameter $T_{\mathrm{c}}(w)$ is considered. This fitting parameter was assumed to be constant and was estimated from the long-time annealing temperature at which the radiation defects disappear [8].

Using the Visual-Fortran programmer the course of the TDF function was calculated and the position of relative minima was determined. The elements proven by APFIM were varied for the calculation. In addition vacancies were taken as potential component in the MCC as vacancies cannot be detected by APFIM. The contents of Fe, Mn and Si in the matrix (x_1, x_2, x_3) are taken from APFIM as the fixed ones. The contents of these elements in MCC (x'_1, x'_2, x'_3) are varied. Furthermore, the vacancy content in the matrix (x_4) and in MCC (x'_4) are also varied. On this way the sum of the contents of the components has equal 100% in matrix as well as in MCC. Thus the minimum of the TDF is found at the space of the variables (x_4, x'_1, x'_2, x'_3).

The calculations show that a relative minimum is only found when

(a) vacancies are not neglected,
(b) a shell model is considered consisting of vacancies-containing MCC core and a highly vacancies-rich (ca. 90%) shell surrounding the core.

As an example in Fig. 1, the cross-sections of the function f (Fe, Mn, Si, vacancy in MCC, vacancy in shell) in the Mn–Si-2d space are plotted for some sets of fixed values of Fe, vacancies in MCC and vacancies in the shell. A relative minimum occurs in all cases. However, the minimum is more pronounced and clearly deeper for the lower Fe content in the MCC core and the higher vacancies content in the shell. Summarizing, the global minimum is found if the content of vacancies is about 37% in the MCC core and is about 91% in the shell. Apart from the vacancies, the core contains Fe, Si and Mn atoms (about 48%, 7% and 8%, respectively). In general, the mean composition of the MCCs corresponds relatively (e.g. without consideration of the vacancies) to the APFIM results [19,20]. The consideration of the surface term in (1) will provide the more accurate determination of the MCC content. However, essential differences in the results are not expected because the composition dependence of the surface tension is low in comparison with the composition dependence of the TDF. For example, the values of σ are 2.0–2.9 J/m^2 for the iron-vacancy binary system and about 0.4–0.5 J/m^2 for the iron–copper binary system under surveillance temperature regimes [25,26]. Therefore one can assume that σ of MCC only change by one order with the composition.

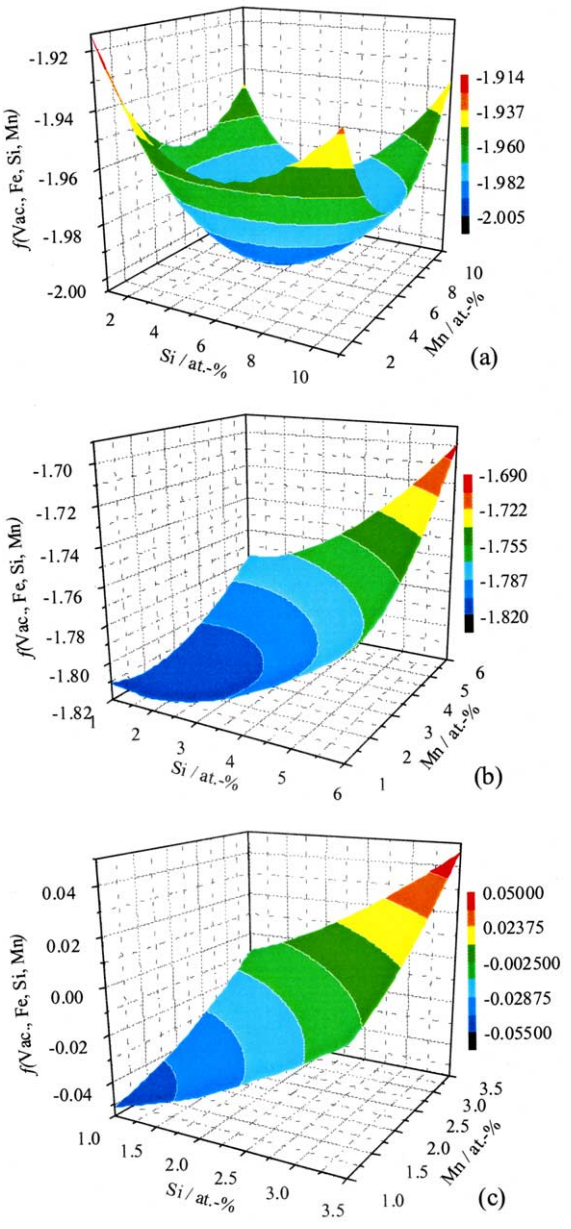

Fig. 1. Cross-sections of the thermodynamics driving force f(vacancies, Fe, Mn, Si) in the Mn–Si two-dimensional space for some fixed content of iron and vacancies in MCC and shell. (a): Fe in core: 54 at.%, vacancies in shell: 85 at.%, (b): Fe in core: 83 at.%, vacancies in shell: 83 at.%, (c): Fe in core: 86 at.%, vacancies in shell: 50 at.%.

3. Small-angle neutron scattering from MCCs

SANS can be used to exact the shell model of MCC, i.e. to estimate the ratio of the size of the core to the shell.

In the following, the magnetic SANS contribution is only investigated. In the case investigated the MCC represents a composite from homogeneous core with a number density of iron atoms $n_{\mathrm{Fe}} = 0.5 n_{0\mathrm{Fe}}$ ($n_{0\mathrm{Fe}}$ = number density of iron atoms in the matrix) and a vacancy enriched shell. The same problem was considered by [27,28] but without complete consideration of the interference between SANS from core and shell. A more accurate procedure has to use the formalism of the pair distribution function [29].

In accordance with Porod's result [29], the scattering factor S (=normalized scattering intensity of a single particle) in case of an arbitrary structure of the inhomogeneity can be calculated using the pair distribution

$$S(L,h) = \int_0^1 p(x) \cdot [(\sin(Lhx)/(Lhx)]\,\mathrm{d}x. \tag{4}$$

Here h is the length of the scattering vector; $p(x)$ is the density of probability to find pairs of atoms in the scattering object on the given distance $d = xL$; $L = 2R$, if the scattering object is a sphere with radius R.

Because the integral of $p(x)$ (=probability $P(x)$) is more suitable for the numerical calculation, Eq. (4) has been transformed by partial integration to Eq. (5)

$$S(L,h) = \sin(Lhx)/Lhx] - [1/(Lh)] \times \int_0^1 P(x) \cdot \{[Lhx\cos(Lhx) - \sin(Lhx)]\}/x^2\,\mathrm{d}x. \tag{5}$$

The pair distribution function $P(x)$ was numerically calculated using a programme on VISUAL FORTRAN in accordance to its definition as ratio of number of pair elements in the sphere volume with distance less or equal to the given $d = xL$. The numerical calculation was executed with steps of $x = 0.00005$ on the range (0; 1) for different sets of the ratio R_c/R (R_c is the radius of the core) and n_{Fe}/n_{0Fe} and compared with $P(x)$ for homogeneous spheres ($P(x) = 8x^3 - 9x^4 + 2x^6$ [29]). The scattering factor $S(L,h)$ was calculated with $P(x)$ obtained by the same programme.

Fig. 2 shows the pair distribution function for some of these sets. In the case of $R_c/R = 0.7$ and $n_{Fe}/n_{0Fe} = 0.5$ the pair distribution curve is almost identical with the curve for a homogeneous sphere with $n_{Fe} = 0$ (magnetic hollow sphere). The resulting course of the magnetic scattering effect for a system of monodisperse spheres also depends on the sphere radius. For the mentioned case there are differences in the scattering curve only for spheres $\geqslant 3$ nm and at scattering vectors $h > 2$ nm^{-1} in comparison with the magnetic hollow sphere.

Finally, the effect of the composite MCC model on the SANS effects which are experimentally expected was estimated. To demonstrate this, in Fig. 3 the reconstructed magnetic scattering curves are shown for different models and compared with the original experimental scattering curve. The example uses the SANS curve measured with a specimen from 10KGNMAA (Russian designation) VVER 1000-type weld material [8]. The material was

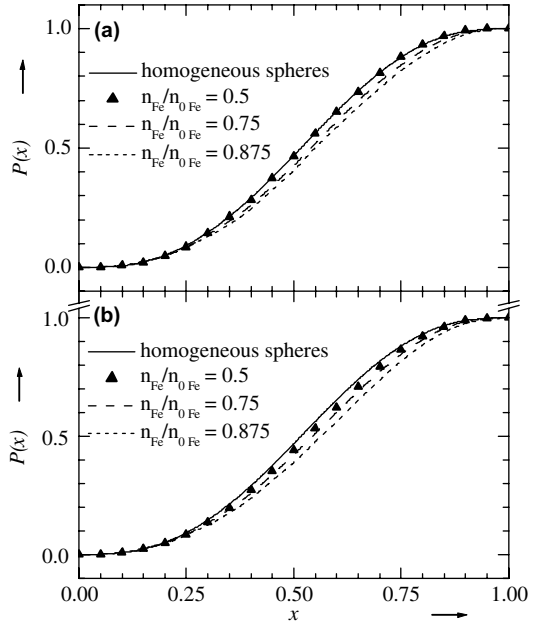

Fig. 2. Pair-distribution function $P(x)$ for the core-shell model and comparison the homogeneous sphere model, (a): $R_c = 0.7R$, (b): $R_c = 0.5R$.

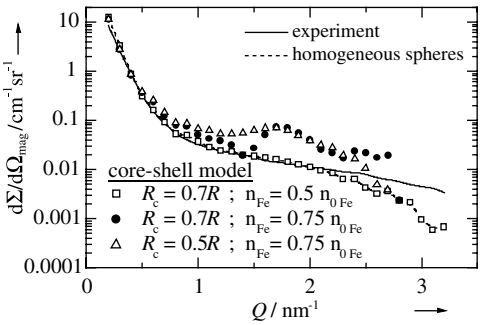

Fig. 3. Comparison between the experimental SANS curve and the SANS curve reconstructed from different particle models.

irradiated up to a fluence of 46.5×10^{18}/cm^2 [$E > 1$ MeV] at 255 °C and shows a clear SANS effect after irradiation in the VVER prototype reactor in Rheinsberg (Germany). The size distribution $D(R)$ was calculated using the indirect transformation method according to Glatter [30] and assuming homogeneous, nonferromagnetic, spherical scattering features. The size distribution curve exhibits a sharp peak near a radius of 1 nm and a low, widely extended maximum between 10 and 16 nm. The ratio of the total SANS intensity to the nuclear SANS contribution (so-called A-ratio) does not depend on the scattering vector and is about of 2.2. Therefore, the presence of the PDC with an A-ratio of 1.4 and CRP with an A-ratio about of 7 is not revealed in the defect nanostructure of the investigated material. Recalculation of the magnetic scattering intensity in Eq. (6)

$$I_m(h) = (n_{0Fe} \cdot b_{fe}^m)^2 \int D(R) \cdot S(2R,h)\,dR, \qquad (6)$$

where b_{Fe}^m is the magnetic scattering length for iron, provides a curve which corresponds to the experimental curve up to the scattering vector h of about 2 nm^{-1}. The scattering intensity in the range of $h > 2$ nm mainly reflects the scattering contribution of very small features ($R < 0.8$ nm). Here is the limit of the resolution of the methods. The calculated magnetic scattering curves in Fig. 3 are also depicted for the core-shell sphere model assuming different values of R_c/R and n_{Fe}/n_{0Fe}, respectively, but the same size distribution function. A ratio $R_c/R = 0.7$ and $n_{Fe}/n_{0Fe} = 0.5$ has the same scattering curve like the homogeneous sphere model without iron. However, relatively low deviations of the ratio of the radii or the Fe content in the core produce clearly different scattering curves. The reason of the strong difference on Fig. 3 in spite of the small differences in probabilities in Fig. 2 is the very fast changing of the function [(sin(Lhx)/(Lhx)] in Eq. (4).

The approach suggested can be generalized in the interpretation of the nuclear SANS. Here, no additional effect is expected. Mn and Si have approximately a nuclear scattering length of the same amount but with the opposite sign (−3.73 fm for Mn, 4.15 fm for Si).

Thus, the nuclear SANS of the MCC only results from the number density difference between MCC and matrix and is similar to the magnetic SANS characteristics. This conclusion is additionally supported by experimental results [8], which show the same h-dependence for magnetic and nuclear SANS.

4. Discussion and conclusion

Radiation raises the lattice defect concentration and, hence, changes the Gibbs energy of the system. This can be connected with the shift of the phase fields or even with the appearance of new phases. Numerical calculations of the negative minimum of the thermodynamic driving forces for a multi-component system, based on the generalization of the approach in Ulbricht et al. [22] for binary alloys, provide stable MCCs composed of a core with about 50% Fe and a very vacancies-rich shell. The calculation used a chemical composition typical for VVER RPV steels and welds and does not contradict the APFIM results on the same material types. Considering that APFIM does not detect vacancies the correspondence with APFIM is rather excellent. Nevertheless, the estimation is only rough as there is a lack of data for the interchange or mixing energies of the distinct components. The used approximation (uniform interchange energy derived from the annealing temperatures of the radiation defects) cannot be really satisfactory. Moreover the consideration of the weak surface tension dependence on the MCC composition can also exact the MCC content.

Depending on the medium Fe content in the core and the size of the shell, the SANS effects of the composite MCCs can agree with the SANS effects of homogeneous, Fe-free clusters of similar size distribution as proven here only for the magnetic scattering contribution. Especially with the result of the thermodynamic estimation, the agreement is very good. However, using conventional SANS experiments, it is not possible to decide whether the scattering defects are homogeneous or composite. More clarification could arise from SANS experiments with polarized neutrons [31].

References

[1] G.R. Odette, Scr. Metall. 17 (1983) 1183.
[2] G.R. Odette, MRS Symposium Proceedings 373, Pittsburgh, 1995, p. 137.
[3] G.R. Odette, G.E. Lucas, Radiat. Eff. Def. Solids 144 (1998) 189.
[4] G.R. Odette, in: M. Davies (Ed.), Neutron Irradiation Effects in Reactor Pressure Vessel Steels and Weldments, IAEA-JWG-LMNPP-98/3, Vienna, 1998, p. 438.
[5] J.T. Buswell, W.J. Phythian, R.J. Mc Elroy, S. Dumbill, P.H.N. Ray, J. Mace, R.N. Sinclair, J. Nucl. Mater. 225 (1995) 196.
[6] S.B. Fisher, J.T. Buswell, Int. J. Pressure Vessel Piping 27 (1987) 91.
[7] G.E. Lucas, G.R. Odette, P.M. Lombrozo, J.W. Sheckehard, in: F.A. Garner, J.S. Perrin (Eds.), Effects of Radiation on Materials: Twelfth International Symposium, ASTM STP 870, Philadelphia, 1985, p. 900.
[8] J. Böhmert, A. Gokhman, M. Große, A. Ulbricht, Nachweis, Interpretation und Bewertung bestrahlungsbedingter Gefügeänderungen in WWER-Reaktordruckbehälterstählen, Forschungszentrum Rossendorf, Wissenschaftlich-technische, Bericht, FZR-381, Juni 2003.
[9] M.K. Miller, S.S. Brenner, Res. Mech. 10 (1984) 161.
[10] J.C. Walmsky, A. Ward, R. Scowen, A.J. Mc Gibbon, J.H. Paterson, Philos. Mag. Lett. 67 (1993) 131.
[11] R.G. Carter, N. Sonoda, K. Dohi, J.M. Hyde, C.A. English, W.L. Server, J. Nucl. Mater. 298 (2001) 211.
[12] P. Auger, P. Pareige, M. Akamatsu, D. Blavette, J. Nucl. Mater. 225 (1995) 225.
[13] M.G. Burke, S.S. Brenner, J. Phys. Colloque C6 47 (Suppl. no. 3) (1986) C2-239.
[14] M.G. Burke, M.K. Miller, J. Phys. Collogue C6 49 (Suppl. no. 11) (1988) C6-283.
[15] M.K. Miller, M.G. Burke, J. Phys. Collogue C6 48 (Suppl. no. 11) (1987) C6-429.
[16] M.K. Miller, M.G. Burke, J. Nucl. Mater. 195 (1992) 68.
[17] P. Pareige, M.K. Miller, Appl. Surf. Sci. 94&95 (1996) 370.
[18] P. Pareige, R.E. Stoller, K.F. Russell, M.K. Miller, J. Nucl. Mater. 249 (1997) 169.
[19] M.K. Miller, K.F. Russell, J. Kocik, E. Keilova, J. Nucl. Mater. 282 (2000) 83.
[20] M.K. Miller, K.F. Russell, J. Kocik, E. Keilova, Micron 32 (2001) 749.
[21] J.W. Gibbs, The Collected Works, 2, Academic Press, New York-London-Toronto, 1928.
[22] H. Ulbricht, J. Schmelzer, R. Manke, F. Schweizer, Thermodynamics of Finite Systems and the Kinetics of the First-Order Phase Transformations, Teubner, Leipzig, 1988.
[23] J.W.P. Schmelzer, J. Schmelzer Jr., I. Gutzow, J. Chem. Phys. 112 (2000) 3820.
[24] R.E. Stoller, in: A.S. Kumar, D.S. Gilles, R.K. Nanstad, E.A. Little (Eds.), Effects of Radiation on Materials: 16th International Symposium, ASTM STP 1175, ASTM, Philadelphia, 1993, p. 394.
[25] M. Smetniansky, De Grande, A. Barbu, Radiat. Eff. Def. Solids 132 (1994) 157.
[26] The SGTE Casebook, Thermodynamics at Work, in: K. Hack (Ed.), Materials Modelling Series, The Institute of Materials, 1996, p. 227.
[27] G. Hilbig, Wissensch Z. der Hochschule für Arch. und Bauwesen (1972) 71.
[28] S. Spooner, Mater. Res. Soc. Symp. Proc. 439 (1997) 489.
[29] G. Porod, Acta Phys. Austriaca 2 (1948) 255.
[30] O. Glatter, J. Appl. Crystallogr. 13 (1980) 7.
[31] A. Wiedemann, BENSC Experimental Report 1999, HMI-B 565 (2000) 303.